Mitotic waves in frog egg extracts: Transition from phase waves to trigger waves

Owen Puls[1°], Daniel Ruiz-Reynés[2,3°], Franco Tavella[1], Minjun Jin[1], Yeonghoon Kim[1], Lendert Gelens[2*], Qiong Yang[1,4*]

[1]*Department of Physics / Biophysics, University of Michigan, Ann Arbor, MI 48109, USA.*
[2]*Laboratory of Dynamics in Biological Systems, KU Leuven, Department of Cellular and Molecular Medicine, University of Leuven, B-3000 Leuven, Belgium.*
[3]Institute for Cross-Disciplinary Physics and Complex Systems (Consejo Superior de Investigaciones Científicas - Universitat de les Illes Balears), Campus Universitat Illes Balears 07122, Palma de Mallorca, Spain
[4]*Department of Computational Medicine and Bioinformatics, University of Michigan, Ann Arbor, MI 48109.*

[°,*] contributed equally

* Correspondence: qiongy@umich.edu; lendert.gelens@kuleuven.be

Abstract

The cell cycle clock network centers on the cyclin-dependent kinase (Cdk1), such that its oscillatory rising and falling activity directs the cell through a series of steps which define one mitotic cycle. When a collection of these oscillators couple, they can synchronize. In particular, early embryogenesis is marked by a series of synchronous and fast cell divisions across the length of the embryo in various systems, e.g. *Drosophila* (approximately 0.5 mm in length) and *Xenopus* (approximately 1.2 mm in diameter). However, the large size of these embryos implies a faster coordinating effect than diffusion can control by itself. Two types of waves have been suggested as a mechanism for such spatial coordination: phase waves and trigger waves, which can be distinguished by both the speeds at which they propagate and the biochemical mechanisms behind their formation.

Here, by using *Xenopus laevis* egg extracts and a Cdk1 FRET sensor to study the time dependence of mitotic waves, we show a transition from phase waves to trigger waves for the first time. We show how the addition of nuclei entrains the system more quickly to the trigger wave regime. We also demonstrate that the system is entrained almost immediately when metaphase-arrested extracts initiate the waves from the boundary. Finally, we complement experiments with computational modeling showing how the observed cell cycle period and wave speed depend on transient dynamics and underlying cell cycle oscillator properties. Our work argues that the transition of fast phase waves to slower trigger waves in the spatial coordination of the cell division cycle occurs as a transient effect due to the time required for trigger waves to entrain the system. Moreover, we argue that trigger waves play a role in spatial coordination, and that

both phase and trigger waves are a manifestation of a common biological process undergoing these transient dynamics.

Introduction

One of the most important processes in all of biology, cell division, is regulated by a well-studied pacemaker oscillator called the mitotic clock which is centered on the activity of the cyclin B-Cdk1 complex (1,2) (Figure 1A). The cell cycle (DNA-replication-division cycle) is defined by the sequence of events by which cells replicate DNA and partition the copies into daughter cells such that each daughter receives precisely one copy of the genome (3).

In early embryogenesis in organisms such as *Xenopus* or *Drosophila*, embryonic cells initially proceed through a series of fast cell divisions (4,5). These mitotic cycles lack many features of mature cells—e.g. gap phases, cell cycle checkpoints, and zygotic gene transcription — which only arise after the mid-blastula transition (MBT) (6) . For this reason, it is key these cycles remain roughly synchronized prior to MBT, even though some desynchronization is tolerated (7). Throughout this process, mitotic events occur within minutes of each other. However, due to the large cell size in such embryos, diffusion alone remains far too slow to coordinate said synchrony: such a process would take multiple hours, not minutes (8–12) .

Previous work highlights the existence of waves of mitotic events — both *in vitro* and *in vivo* — which propagate at speeds sufficiently high (~0.04-0.06 mm/min) to communicate across the lengths of the embryo (8,9). First, trigger waves — resulting from the coupling of diffusion and local dynamics (10,11) — were shown to coordinate mitosis in *Xenopus,* using nuclear envelope breakdown (NEB) to illustrate their propagation after a few early, largely synchronous cycles (8) . Subsequent work illustrated that the nucleus itself serves as the pacemaker for said waves, locally accelerating oscillations possibly by aggregating cell cycle regulators and thus driving waves (13,14). The aggregating mechanism was later confirmed in individual oscillating microemulsions (15). Trigger waves, however, are seemingly not the end of the story.

Much like *Xenopus* and other metazoans, the fruit fly embryo undergoes a series of rapid, roughly synchronous syncytial nucleus divisions post-fertilization (6). However, *Drosophila* embryos display waves of mitotic completion that traverse the entirety of the embryo (hundreds of microns) in mere minutes at early stages, speeds much faster (~0.1 mm/min) than what could be achieved by traditional trigger wave models (9). Moreover, embryos display distinct spatial dynamics which forgo the classical picture of a stable regime invading into and promoting a metastable regime (10,11). Instead, spatial gradients in Cdk1 activity are largely preserved, while the overall levels are swept upwards (16) .

Vergassola, et al. propose that a distinct phenomenon termed “sweep” waves (“phase” waves in our terminology, terminology accepted by the authors in a subsequent review (12)) is responsible for the ultra-fast waves observed *in vivo* (12,16). Phase waves appear to spread due to local phase gradients but are not actively spread by mutual interactions, in contrast with trigger waves which do propagate through a coupling of diffusion and local reactions (8–12). The authors propose that a time-dependent sweeping-up of Cdk1 activity leads to wave-like behavior spreading at scales faster than trigger waves, consistent with phase waves. Interestingly, the authors observe that the period of the oscillator lengthens for late cycles (due to Chk1) and propose that phase and trigger waves might be linked through this mechanism (16). In more recent work, the authors speculate that such a transition could also exist in *Xenopus* and called for direct measurements of Cdk1 activity to resolve this open question (17).

In this work, we present the first direct evidence of mitotic waves in *Xenopus* using a FRET sensor for the ratio of Cdk1 activity and its opposing phosphatase. We show that waves of Cdk1 activity can form spontaneously in absence of the nuclear pacemaker, sharing the fundamental nature of the classical

chemical waves in a Belousov–Zhabotinsky (BZ) reaction-diffusion system. With this, we investigate the time-dependent behavior of mitotic waves in *Xenopus* extracts, showing a transition from phase-wave-like to trigger-wave-like patterns over time, and as a result, offer the connecting thread for these phenomena. We also probe the role of nuclei in wave propagation, showing that in addition to acting as pacemakers, nuclei entrain the system to the trigger wave regime. Stemming from lessons learned in these experiments, we then propose a novel method for generating directed waves *in vitro*¸ a setup which reinforces the notion of entrainment explicitly. In short, we use a reservoir of active Cdk1 to drive waves through an oscillating bulk. Taken together, we offer a generalized picture of the interplay between phase and trigger waves and their role in the spatial coordination of *Xenopus laevis*' early embryogenesis.

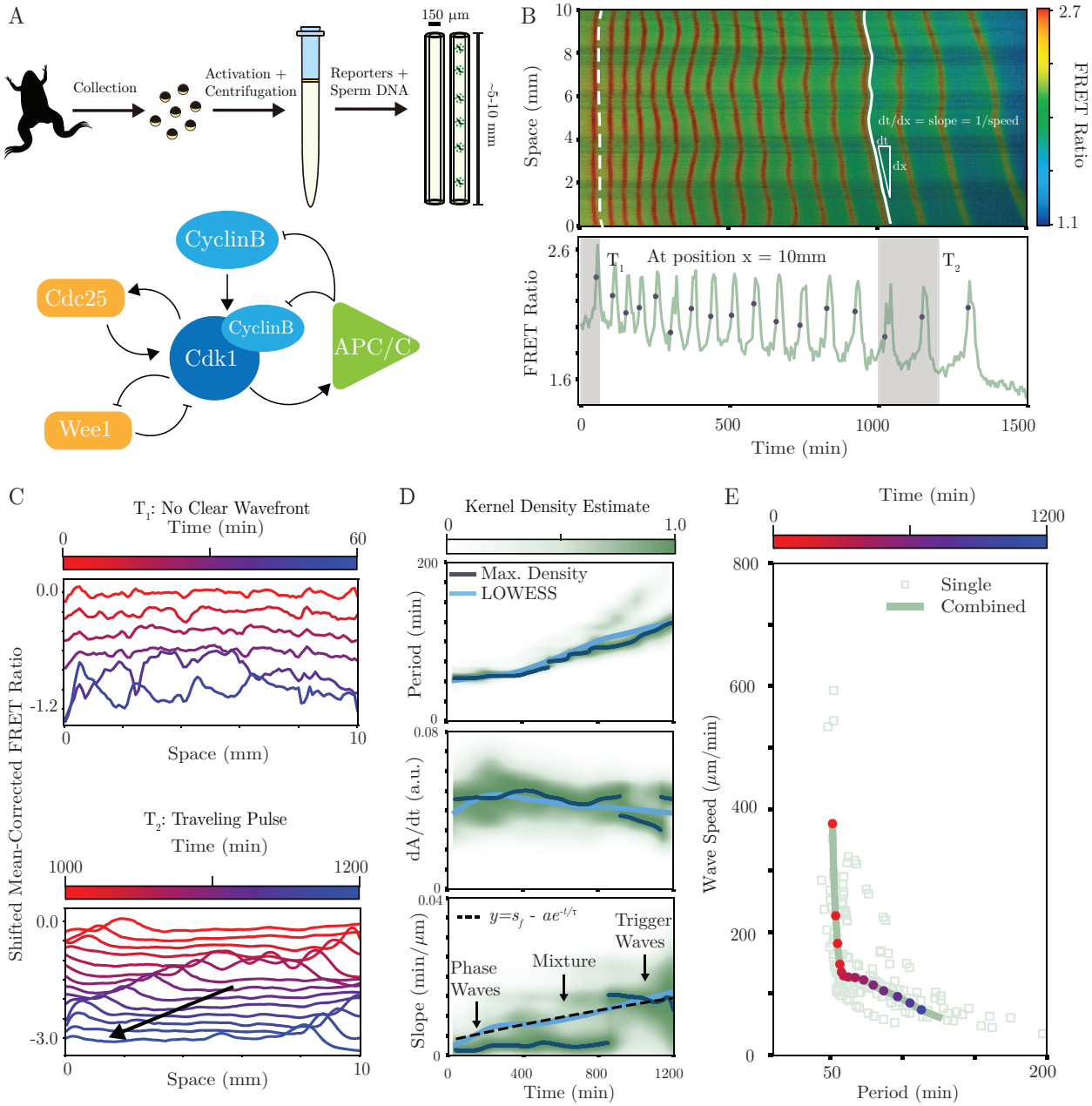

Figure 1: Temporal dependence of mitotic wave dynamics. (A) Top: Schematic view of the experimental preparation of cycling cell-free extracts using Xenopus laevis frog eggs loaded in Teflon tubes 10 mm long and 150 µm in diameter. Bottom: Schematic representation of the regulatory network driving the mitotic clock. (B, C) The activity of cyclin B-Cdk1 is reported using a Cdk1 FRET sensor indicated with the color bar. In white the detection and characterization of wave profiles is indicated (dashed for phase waves at early times, solid for late-time trigger waves). The temporal evolution of the FRET ratio signal is shown in the bottom panel for the position x=10mm in green indicating with purple

points indicating the time of maximum time derivative per cycle. The derivative itself is not shown. The gray regions correspond to time ranges used in panel C for the visualization of the Mean-Corrected FRET signal colored with time showing in-phase activation (top) in contrast with traveling pulse activation (bottom). (D) shows the temporal evolution of the period, time derivative, and slope (or inverse of the wave speed) measured locally using the normalized kernel density estimation to determine the probability distribution normalized at each time indicated with green colormap. The maximum density (dark blue) and the locally weighted scatter plot smoothing (LOWESS, light blue) are depicted. (E) Local measures of the period and wave speed are represented with green squares. The dispersion relation is computed by combining the LOWESS estimations of speed and period (green line) and dots indicate time according to the colorbar.

Results

Mitotic waves transition from fast phase waves to slower trigger waves

We set out to characterize mitotic waves in cycling extracts (no sperm DNA – no nuclei) using the FRET sensor. As this sensor indicates the activity of Cdk1 over time, it allows us to visualize waves of the mitotic state directly for the first time in *Xenopus*, instead of relying on down-stream events such as NEB. Taking this one step further, these wavefronts – as defined by the profiles of maximal activity – can be analyzed directly for instantaneous wave speed along each curve, rather than assuming a constant speed for each front defined near the source. Moreover, time traces of the activity at single positions in space (x-slices) facilitate the measurement of biochemical properties such as activation rate, and cell cycle properties such as period, etc.

A representative kymograph for such an experiment is shown in Figure 1B to introduce the relevant quantities. For presentation purposes, we present the FRET signal as a heatmap with cool colors corresponding to low Cdk1 activity, and warm colors similarly for high activity (Figure 1B). The explicit time evolution of the FRET donor-to-acceptor ratio is also given for a small slice (at position x = 10 mm; Figure 1B, Bottom). Peaks in this signal are what allows us to cluster wavefronts (Figure 1B, White trace). Visually, one can observe a difference between early time patterns — largely synchronous and/or fast moving (roughly vertical dashed line, as indicated) — and later patterns — linear fronts (solid line of finite slope) — resembling that of trigger waves. The speed of these patterns is measured by taking the instantaneous derivative (dx/dt) of the interpolated wavefront (Figure 1B). We choose to measure the slope (inverted speed, dt/dx) as the speed of early time patterns is often infinite at this resolution. Periods (peak-to-peak) are also measured from these signals and are given in Figure 1D. Additionally, we calculate the maximal time derivative of the activity (dA/dt) for each cycle. The purple points in Figure 1B (Bottom) represent these maxima for this kymograph, at that slice.

We observe clear changes in spatial profiles over time. At early times, the patterns we observe resemble phase waves highlighted in *Drosophila* embryos (Figure 1C, Top). Taking a cue from Hayden et al. (17), when we plot the FRET ratio spatial profile over consecutive frames for early cycles, we see a roughly uniform upswing in activity, with local peaks preserved, largely preserving spatial gradients (Figure 1C, Top). While this does not equate to a strict proof for the existence of sweep waves in *Xenopus*—higher time resolution and parameter scaling are required to be certain—the similarity is striking. Conversely, at late times (1000-1200 min), the system exhibits clearly linear, trigger-wave-like fronts, characterized by traveling pulses (Figure 1C, Bottom). This implies a transition from phase waves at early, fast cycles, to trigger waves at late, slower cycles.

To quantify this transition, we study how period and slope change over time by aggregating different experimental realizations (N = 6) of the kymograph presented in Figure 1B (normalized kernel density

estimates [KDE]). From both the kymograph and the FRET ratio trace, one can identify the typical period lengthening due to a noticeable increase in interphase. This trend matches what is observed in extracts generally (13,18). We observe a roughly linear increase in the period over time, as indicated by the locally weighted scatterplot smoothing (LOWESS) curve (Figure 1D, Top). We hypothesized that this may be accompanied by a decrease in the speed of activation, dA/dt, and a shift away from relaxation dynamics. To test this, we calculated the maximal derivative between wavefronts at each point, for each cycle. As can be seen in Figure 1D, Middle, this quantity remains fairly constant, or slightly decreasing, over time.

For wave speeds, the slope generally increases over time, corresponding to a slowing of the speed (Figure 1D, Bottom). In particular, at late times, the KDE maximum abruptly shifts to larger slopes (from 0.001 to 0.02 min/μm), indicating a transition to trigger waves (Figure 1D, Bottom). The smoothed data does not display an abrupt transition, suggesting this represents a gradual movement towards trigger waves as the dominant behavior. We quantify this movement by fitting a decay function to the smoothed data to extract the entrainment time τ (Figure 1D, Bottom, Dashed Line). This value gives us an estimate for how long it takes the system to primarily exhibit slow trigger waves. For this data, $\tau > 1500$ min (extract death), suggesting that trigger waves do not completely dominate the system, even at late times.

When combined, these measurements reveal a monotonically decreasing relationship between the wave speed and the cell cycle period (Figure 1E). At early times, the period is short, and the system exhibits phase waves of speeds much faster than trigger waves. However, these transients eventually die off as the system transitions to a regime quasi-dominated by trigger waves (Figure 1D). This speed-period relation also appears to confirm what Hayden et al. report regarding a sweep-to-trigger transition, though in time, in this case (17). As a result, our results offer the first quantification of the time-dependent behavior of mitotic waves in *Xenopus laevis* egg extracts and bridge our understanding of mitotic waves between different model systems at different time scales.

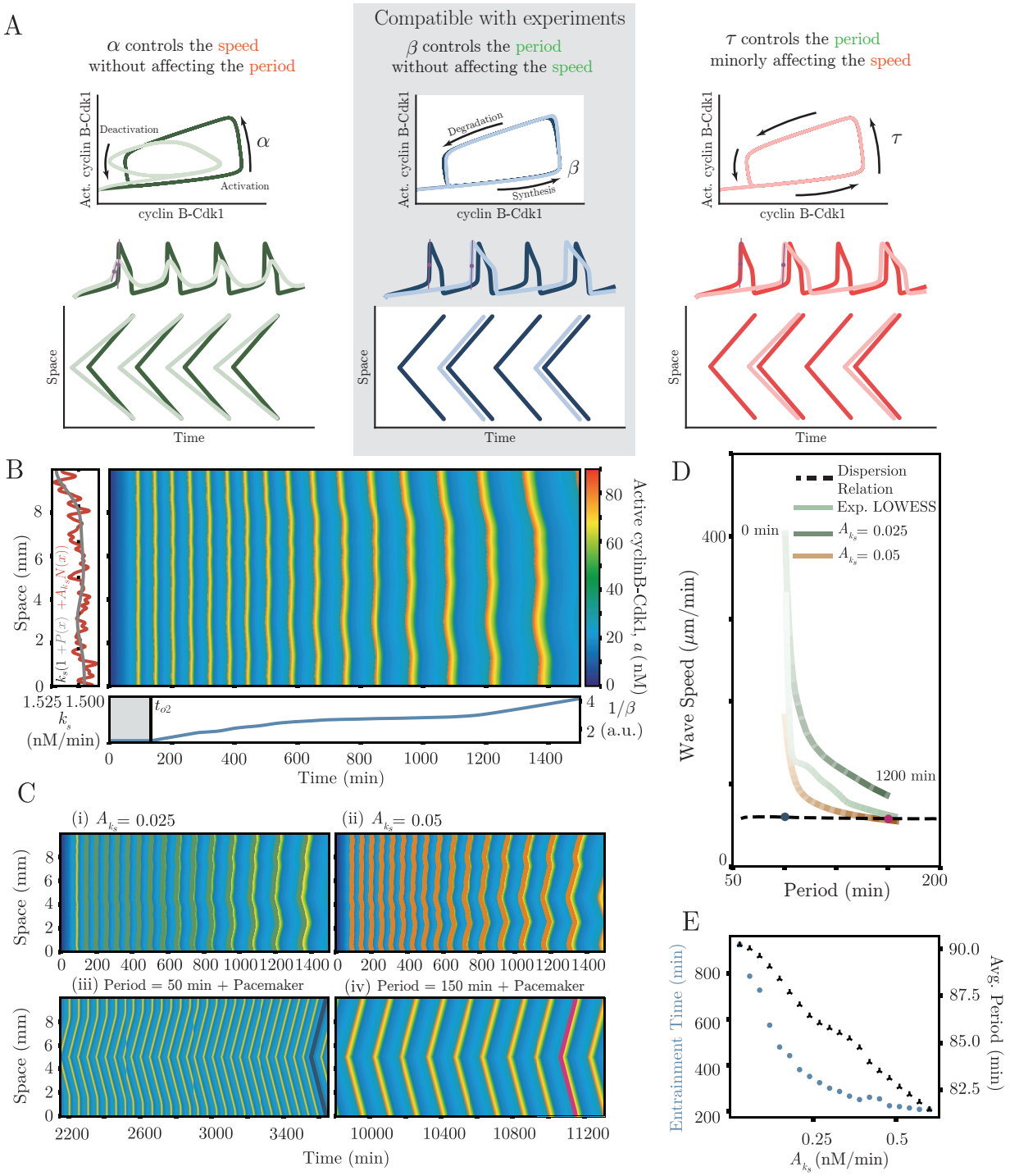

Figure 2: Mathematical modelling explains the transition from phase to trigger waves. (A) Schematical representation of the effects on the period, $\frac{dA}{dt}$ and wave speed decreasing timescale separation with α (left), decreasing synthesis and degradation rates with β (center), and all rates with τ (right), see quantitative analysis in Fig. S2. (B) Spatiotemporal evolution of the activity of cyclin B-Cdk1 showing the transition from phase to trigger waves incorporating the experimental dependence of the period with time using the parameter $\beta(t)$ (bottom) and spatial variability in the synthesis term $k_s(x)$ (left, see details in Methods). (C) Influence of spatial heterogeneity on the entrainment by trigger waves by increasing the amplitude of the synthesis around the average value A_{k_s} (i - ii) and by introducing a pacemaker with different period at the center of the spatial domain and increasing the background period (iii - iv). (D) Dispersion relation of the experimentally measured values (light green), of the numerical simulations in panel C (i, green, ii, yellow) and the theoretical dispersion relation using the parameter β to scan the period (black dashed line) where the numerical simulations in (ii) and (iv) are indicated with blue and purple dots respectively. (E) Dependence of the entrainment time measured using an exponential fit and average period as a function of the amplitude of the synthesis around the average value A_{k_s}.

A generic cell cycle model shows that transient dynamics explains the observed phase to trigger wave transition

The observed transition from fast phase waves to slow trigger waves could be the result of two contributing factors. On the one hand, we observe a lengthening of the oscillator's period, suggesting a change in the system's properties over time. On the other hand, as in any oscillatory medium, emerging waves require a finite amount of time (transient time) to form traveling waves. Therefore, we turn to mathematical modeling to quantify the contribution of the two effects (period and transient time) on the observed change in wave speed. We use a mathematical model introduced by Yang and Ferrell (19) and later extended by Chang and Ferrell (8) to describe mitotic waves. The model describes the activity of the complex cyclin B-Cdk1 in its active form (noted as a) and its total concentration (noted as c). Cyclin B is synthesized at a rate k_s and then it rapidly binds to Cdk1. The activity of the cyclin B-Cdk1 complex is regulated by the phosphatase Cdc25, which activates the complex by dephosphorylation, and the kinases Wee1 and Myt1, which deactivate the complex by phosphorylation. Finally, high Cdk1 activity leads the anaphase-promoting complex / cyclosome (APC/C) to target cyclin B for degradation (Figure 1A, bottom and Eqs. 1-2). The rates of activation, deactivation, and degradation are described by ultrasensitive response curves dependent on the activity of cyclin B-Cdk1 (a) and parametrized using experimental measurements (19).

To study the contribution of period lengthening on the transition from fast to slow waves, we analyze how the model responds to parameter changes. As a result of the activation and inactivation processes, the model has a bistable switch at its core and exhibits relaxation oscillations with two different time scales. During cyclin B synthesis, the system slowly progresses through interphase. However, when a threshold value of total cyclin B-Cdk1 complex is reached, the oscillator transitions to its active state on a much shorter timescale. If diffusion is incorporated into the model, a rich set of spatially extended dynamics emerges such as coherent oscillations, excitability, spiral waves, and traveling waves. Following a similar approach to that of Rombouts and Gelens (20,21), we explore the speed-period relation of traveling waves to investigate the dependence of wave speed, period, and activation rate $\frac{da}{dt}$ to changes in the underlying parameters of the model. The dependence of this speed-period relation with model parameters can be better understood by using three different scalings parametrized by α, β, τ (Figure 2A). The parameter α scales the rates involved in the activation and inactivation process; as a result increasing α increases $\frac{da}{dt}$ and the wave speed while the period remains almost constant (Figures 2A and S2 left). The parameter β scales the synthesis and degradation rates of cyclin B leading to a modulation of the period associated with interphase and mostly unchanged values of wave speed and $\frac{da}{dt}$ (Figure 2A and S2 center). Finally, decreasing τ corresponds to a global time scaling affecting all the rates in Eqs. 1-2, which increases the period, decreases $\frac{dA}{dt}$, and decreases the wave speed (Figure 2A right). Equivalently, scaling τ can be interpreted as a combined scaling of α and β (see Fig. S2). In this context, the simplest explanation for the observed transition from fast phase waves to slow trigger waves (Figure 1D) is given by a decrease of β over time (Figure 2A center). Decreasing β will increase interphase while keeping $\frac{da}{dt}$ almost unchanged. However, the change in wave speed is not sufficient to fully reproduce our experimental observations.

To quantify the effect of transient dynamics on the transition from phase to trigger waves, we perform numerical simulations incorporating the temporal dependence of the period captured by the LOWESS curve by changing β accordingly. Additionally, we introduce a noisy profile of synthesis rate $k_s(x)$ in space to account for spatial heterogeneity (see details in Methods). Heterogeneous synthesis will induce regions with smaller local periods that will act as pacemakers emitting waves. Diffusion rate, which strongly influences wave speed, ranges around 600 $\mu m^2/min$ for proteins of a similar size to the complex cyclin B-Cdk1 (8). Here, we used 240 $\mu m^2/min$ to reproduce the wave speed at the end of extract lifetime ($\gtrsim$ 1000 min), which is compatible with previous experimental results in the fly embryo (9). Then we apply the same wave analysis used for the experimental characterization of mitotic waves *in vitro* to our in silico modeling and represent the speed-period relation together with the experimental curve (Figure 2D).

The transient regime in which pacemakers gradually entrain the system leads to the observed change in wave speed. Initially, phase waves dominate until regions oscillating with higher frequency entrain the whole spatial domain by sending out trigger waves. This transient effect can be controlled by increasing the amplitude of the heterogeneity A_{k_s} with respect to the average value, which strongly reduces the entrainment time as shown in Figure 2D, E. In support of these findings, we suppress the slowing down of the period and still observe the same transition from phase to trigger waves (see Supplementary Figure S1). While the period dependence likely contributes to reducing the wave speed, the big change in speed from > 300 to ~50 $\mu m/min$ can not be explained by the period slowing down alone. As a matter of fact, wave speed only marginally decreases with increasing period when β is decreased, as shown by the theoretical speed-period relation in Figure 2D, black dashed line. In conclusion, the transition from fast phase waves to slow trigger waves can be mostly explained through the finite time required by traveling waves to establish themselves (transient time) because period lengthening alone cannot reproduce our experimental observations.

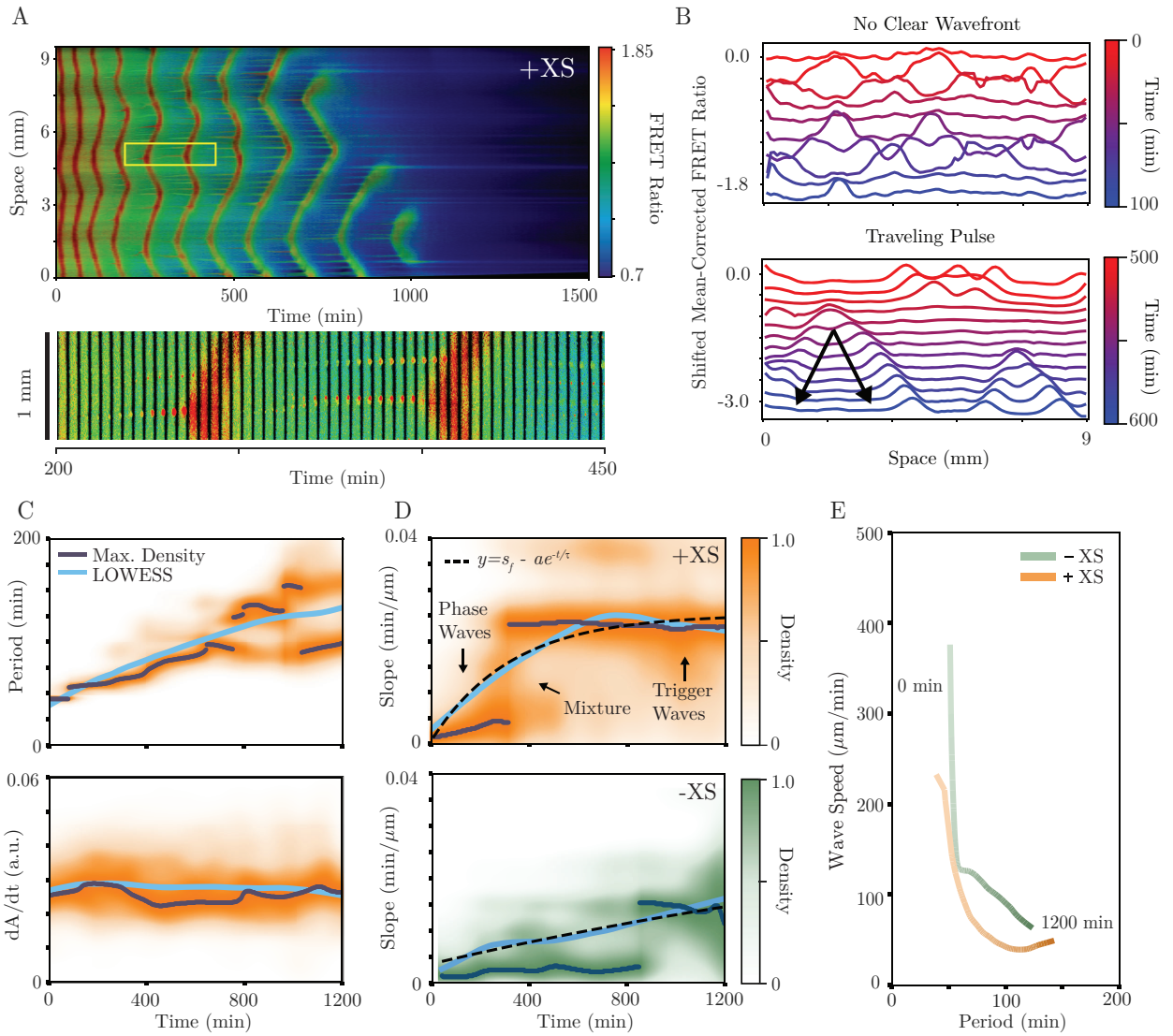

Figure 3: Nuclei entrain the system to the trigger wave regime. (A) Representative kymograph of the effects of adding sperm DNA (+XS) showing the formation of nuclei. A magnified view of the region inside the yellow rectangle is provided in the lower panel with high FRET ratio (in red) revealing nuclear growth before the entry into mitosis. (B) Comparison of Shifted Mean-corrected FRET Ratio at early times with no clear wavefront (Top) and distinctive traveling pulses at late times (Bottom). (C) Time dependence of period and $\frac{dA}{dt}$ using the normalized kernel density estimate according to the orange colormap, overlying the maximum density (dark blue) and LOWESS (light blue). (D) Comparison of the time dependence of the slope for the case of added sperm DNA (+XS, orange) and control (-XS, green) using the same measures as in panel (C). (E) Dispersion relation for the two conditions (±XS) reveals a faster entrainment when nuclei are present.

<u>Nuclei speed up the transition from phase waves to trigger waves</u>

However, this also poses the question: how does this transition change, if at all, when the system is perturbed in such a way that the transient time is altered? Specifically, as discussed, nuclei appear to play some role in wave formation by acting as pacemakers (13,14). Modeling work demonstrates that explicit and implicit inclusion of pacemakers drives waves at the pacemaker frequency, and that the corresponding wave speed depends on this driving frequency (8,13,20–22). This suggests that compartmentalizing the cytosol and/or introducing pacemakers might affect how the system transitions over time. The question then becomes, if present, how can we characterize this change?

To answer this question, we reconstitute nuclei by supplementing extracts with demembranated sperm DNA (+XS), as done before in the field to study mitotic waves (8,13–15). The FRET sensor contains

an NLS-tag, meaning it will report the activity within the nuclei, but also the behavior of Cdk1 post-NEB. A representative kymograph is given in Figure 3A, and the zoomed-in inset (Figure 3A, Bottom) shows individual nuclei that form during interphase and import active Cdk1 prior to NEB. Furthermore, even at a relatively coarse timescale, the pacemaker nucleus imports and contains more active Cdk1 earlier than its neighbors, as expected (Figure 3A, Inset). After NEB, active Cdk1 fills the local region and pulse-like waves propagate as usual (Figure 3B, Bottom). As in the case without sperm DNA, the spatial profiles clearly indicate propagating pulses (Figure 3B, Bottom). Similarly, at early times, the patterns in the sperm-DNA-supplemented conditions resemble those in experiments without. That is, despite nuclei visibly forming, we observe a comparable sweeping up of activity, though the effect is much noisier and punctuated by peaks associated with the nuclei themselves throughout the tube (Figure 3B, Top). Although the *Drosophila* embryo also contains nuclei, as it is syncytial, previous studies have not explicitly investigated the effect of nuclei on mitotic waves (16), making it difficult to compare spatial profiles across the two systems.

Regardless, repeating the same workflow described previously to this compartmentalized system, we find qualitatively similar behavior for each of the relevant quantities: the period and slope both increase over time, while dA/dt is again constant (Figure 3C, D). However, while the periods do not differ significantly between the two conditions, namely +XS (Figure 3C, Top) and -XS (Figure 1D, Top), the slope for these waves containing nuclei reached a persistently higher level than that measured for tubes without nuclei within the observation time window of 1200 min (Figure 3D), suggesting the presence of nuclei may impose an impact on the time-dependent properties of wave propagation. To quantify this, we again measure the entrainment time. Unlike before, τ = 290 ± 10 min, indicating the nuclei contribute positively to the development of trigger waves. Interestingly, both fits produce a plateau slope around 0.025 min/μm (40 μm/min) implying similar long-period behavior and agrees with speeds previously reported (8,13). This discrepancy is made all the clearer when considering the speed-period relation. As shown, the transient phase waves give way to trigger waves much more rapidly than in the systems without nuclei, as indicated by the quicker decay in speed (Figure 3E). Again, the reader should equate the movement towards longer periods with the forward progression of time, as indicated by increasing color darkness with time (Figure 3E). The slight increase at late times is likely due to extract death. Despite this, it is clear the addition of sperm DNA (nuclei) causes the system to admit trigger waves earlier in time, but also “earlier” in period, suggesting speed and period are largely independent (Figure 3E). This reinforces the idea of speed changing due to transient effects, rather than being driven by changes in period.

To summarize, we consider this phenomenon to represent the nuclei entraining the system to the trigger wave regime: this perturbation manifests as entrainment. As mentioned in the introduction, previous work(s) identified nuclei as the pacemakers of mitotic trigger waves (13,14). In that sense, the nuclei offer a nucleation point for singular wavefronts. In light of our work here, we extend this notion to argue that the nuclei perform a global role of bringing the system out of the transitory, less-specified phase wave regime and into the well-defined, classical trigger wave regime. To be complete, these data generally follow the trends we and others in the field observed in past work. In systems without nuclei, patterns remain diffuse and exhibit fast speeds. Over time, trigger waves do develop, albeit slowly. Conversely, systems with nuclei develop trigger waves early and often. The result, in terms of measurables, is that the former display fast speeds that slowly decrease, while the latter display speeds that quickly decay and follow a trigger wave speed-period relation.

Phase waves quickly transition to trigger waves when cycling extract is in contact with a cytostatic-factor extract

To confirm and reinforce this notion of entrainment in mitotic waves, we focus on driving waves explicitly. To accomplish this, we take inspiration from published work on driving apoptotic waves *in vitro*: the authors utilized a reservoir of extract arrested in apoptosis (cell death) to drive an apoptotic signal through a tube filled with extract arrested in interphase (23) . They distinguished between reservoir material diffusing into the tube using a fluorescent dye and the resulting apoptotic wave. We reasoned that we could accomplish something functionally similar but with cycling extract.

The reservoir in question is cytostatic-factor (CSF) extract (also called metaphase-arrested extract) which is derived from inactivated embryos arrested at meiosis-II (24,25). The biological details of CSF arrest remain somewhat in question, though the field largely agrees most signs point to the Emi family of proteins serving a critical role through their inhibition of APC/C (Figure 4A), with possible additional function provided by the Mos-MAPK pathway (26,27). Regardless, CSF extracts exhibit and maintain high Cdk1 activity unless released from arrest by treatment with Ca2+ as we do in the cycling extract protocol (28). Moreover, these extracts can be reliably frozen and stored for many months, giving us a reliable source of stable high-activity extract (29). Due to the self-promoting activity of Cdk1 in the mitotic circuit, supplementing oscillating extract with CSF ought to result in forced activation and resulting traveling mitotic waves.

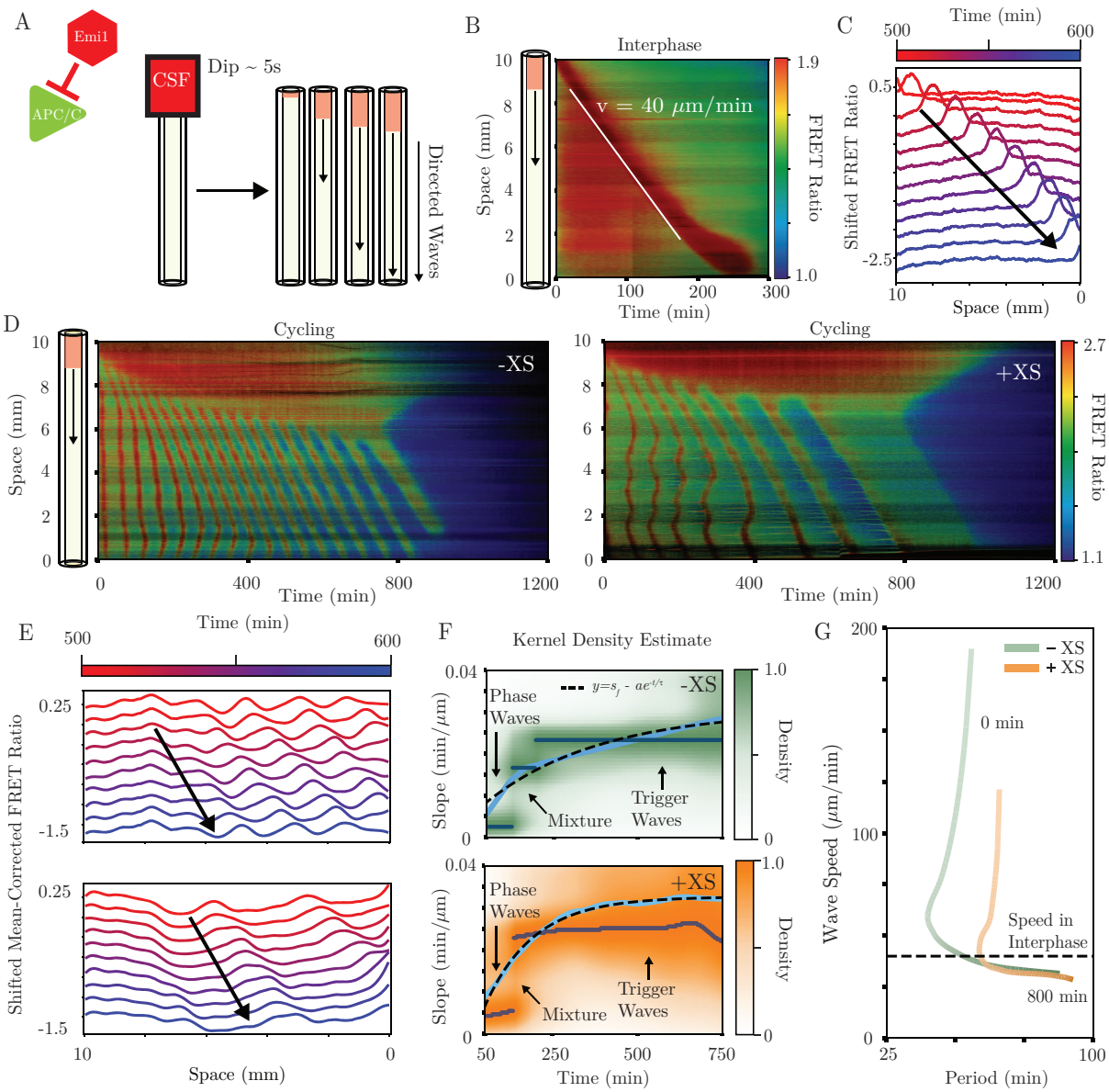

Figure 4: CSF boundary-driven mitotic waves. (A)Schematic representation of the mechanism maintaining high Cdk1 activity in CSF extracts by Emi1 mediated APC/C inhibition and experimental setup to trigger boundary-driven mitotic waves by a 5 seconds dip in CSF extract. (B) Solitary pulse of high Cdk1 activity propagating in an interphase arrested extract triggered using the experimental procedure in (A). (C) Spatial profiles of the shifted FRET ratio from the kymograph in B showing the excitable pulse. (D) Boundary-driven travelling waves without (-XS) and with nuclei (+XS) present. (E) Travelling waves revealed by the Shifted Mean-Corrected FRET ratio at early and late times. (F) Comparison of the time dependence of the slope for the two conditions in panel (C). (G) Dispersion relation combining the LOWESS estimations of the period and speed for conditions with and without nuclei (±XS).

As a proof of concept, we first validate this setup by creating a bistable traveling wave, using CSF extracts, where Cdk1 activity is arrested at a high stable state, to excite a traveling pulse of Cdk1 activity in interphase extracts, where Cdk1 activity is at a low stable state. In principle, dipping an interphase-extract-filled tube into a CSF reservoir should produce a singular wavefront emanating from the source region. To do so, interphase extracts are prepared using the standard protocol in the field (30). Interphase extracts are loaded into Teflon tubing and dipped into a reservoir of CSF. Interestingly, for the first time, we experimentally observe a single traveling pulse connecting a high Cdk1 activity with a low Cdk1 activity propagating from the dipped end of the tube (Figure 4B). These fronts consistently propagate at 40 ± 2

μm/min, showing a very similar velocity of previously measured mitotic trigger waves in cycling extracts (8,13,14). This experiment also demonstrates the efficacy of this system setup.

Turning to waves in cycling extracts, the mitotic arrested region persistently drives waves of Cdk1 activity throughout the tube both with and without added sperm DNA (Figure 4D). As in the undriven experiments with the FRET sensor, wavefronts appear as pulses of high Cdk1 activity (Figure 4E). Importantly, the pulse-like nature of the fronts confirms them as trigger waves. It is noteworthy to see the dominance that the driving exerts on the system, and it highlights the efficacy of trigger waves at disseminating biological information over large distances. Applying the same analysis workflow as before, we again observe that the oscillation period slightly decreases initially, likely due to the diffusing influence of CSF to rapidly increase over time (Figure 4G). Focusing on the addition of sperm DNA, the observed behavior is qualitatively similar, though the magnitude of the periods is initially different (50 and 70 min for -XS and +XS, respectively) (Figure 4G). In this case, despite experiencing the same driving force, the induced period was longer for tubes containing nuclei (Figure 4G).

When measuring the wave speed, we observe two main phenomena. First, slopes for the systems with nuclei remain higher than their non-nuclei counterparts, matching what we observed in the non-driven system (Figure 4F,G). This is likely due, in part, to the longer periods we observe, but also suggests a possible difference in the systems at the level of wave propagation. Calculating the entrainment time as before, we find the entrainment time for data with nuclei (150 ±10 min) remains shorter than that without (300 ± 10 min) (Figure 4F). This could point to some cumulative effect from multiple pacemakers: both the CSF and nuclei contribute to the entrainment. Regardless, both entrainment times are significantly faster than their undriven counterparts (Figure 4F, ±XS, as compared to Figure 3D, ±XS). Interestingly, the entrainment time for the CSF-driven case without nuclei (+CSF/-XS, 300 ± 10 min) is still slightly longer than the undriven case with nuclei (-CSF/+XS, 290 ± 10 min). It is plausible a set of multiple, but theoretically weaker, pacemakers could entrain the system faster given a distributed effect throughout space. Future work could probe this effect more carefully. Additionally, the fitted slope = 0.03 min/μm closely matches what we and others observed previously (8,13,14).

Importantly, driving the system in this way explicitly entrains the system to the trigger wave regime, quickly and permanently (Figure 4F, G). The phase waves of early times quickly—within two or three cycles—give way to trigger waves which propagate across the entirety of the tube. These waves appear to follow a clear speed-period relation, distinct from the undriven case (Figure 4G). In this way, driving the system elucidates a clear difference between the transients—and possible phase waves—of early times and trigger waves, and reinforces the notion of entrainment explicitly.

<u>The presence of phase waves and trigger waves depends on spatial heterogeneities in initial conditions and system parameters</u>

A fundamental difference conceptually separates phase waves from trigger waves. While information transmission by phase waves is nearly absent and synchrony is only maintained when the initial phase difference is small, trigger waves transmit information over long distances. The mechanisms underlying the two kinds of waves is also different, both appear in systems that are oscillatory, but a trigger wave requires time-scale separation and spatial coupling commonly mediated by diffusion. Time-scale separation in our experiments is naturally present due to the rapid activation time of cyclin B-Cdk1

compared to cyclin buildup due to synthesis. It is this rapid activation that excites neighboring regions through protein diffusion and triggers a sustained propagation of the wave. In contrast, phase waves appear as a result of a small delay in the activation time between different positions, creating a structured phase difference which takes the appearance of a wave.

Another important difference is in the speed of the wave and its stability; the speed of a trigger wave is uniquely defined because of properties of the underlying oscillator and diffusion and is said to be stable because a wave with different propagation speed will converge to the stable one. Conversely, a phase wave is not stable, it can appear at any speed, and diffusion will attenuate phase differences with time until the system oscillates synchronously.

To show these phenomena, we use numerical simulations to initiate a trigger wave by introducing a period difference $\tau(x)$ at the central position of the spatial domain with spatially homogeneous levels of activity as initial condition. In contrast, we initiate a phase wave by keeping the period fixed in space and using an initial condition where there is a linear difference in the phase of the oscillator that decreases as one moves far from the central position (see Figure 5A). Then we explore the robustness of the two kinds of waves by reducing the time-scale separation of the oscillator using the parameter α. Figure 5 clearly shows how trigger waves propagate in space in a stable manner entraining the oscillatory background only when the oscillations are relaxation-like ($\alpha = 1$). Quantifying the speed of the wave with the fit $x = d + vt^{\gamma}$ in Figure 5C shows that low values of α, which correspond to sinusoidal oscillations, lead to a curved front resulting from the impossibility of the wave to properly form and a value of γ bigger than one, while for increasing α the wave shows a linear front and γ approaches one. Increasing timescale separation with α also amplifies the penetration depth of the wave into the medium (20,21). Measuring the evolution of the wave speed the value converges to the stable trigger wave speed, while the speed of the phase wave increases with time as the oscillations synchronize (Figure 5B). Additionally, the formation of a phase wave at initial times is not affected by the time-scale separation.

Hence, as observed experimentally and confirmed with numerical simulations in Figure 2, spatial heterogeneity in initial conditions will initially induce phase differences that will appear as phase waves. When those heterogeneities are strong enough and maintained, trigger waves are also initiated that will entrain the system and dominate in the long term (after a transient time).

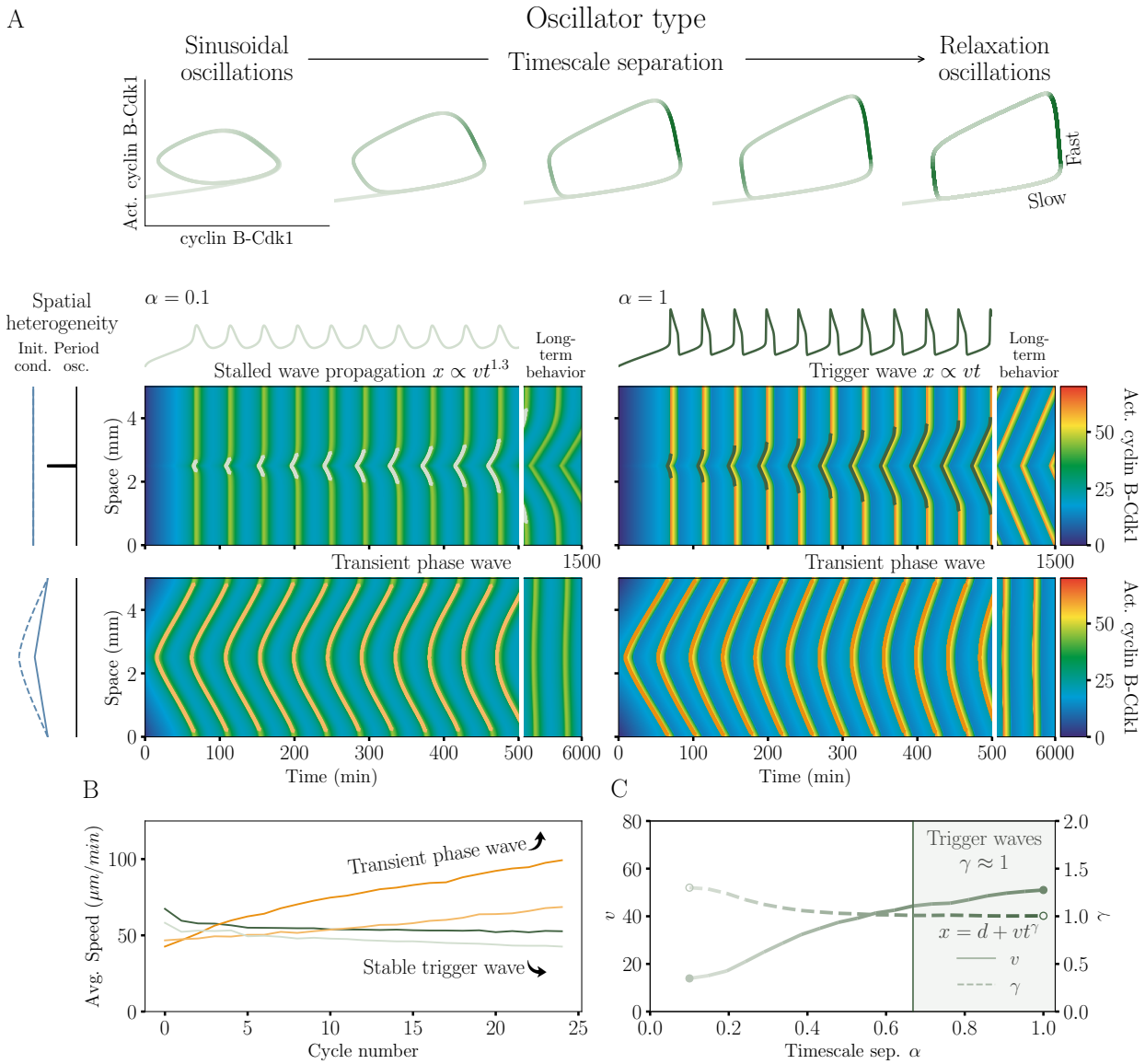

Figure 5: Influence of the oscillator and spatial heterogeneity in the formation of phase and trigger waves. (A) Phase plane trajectory for different oscillators by increasing timescale separation from left to right (Top). Time series for the values of $\alpha = 0.1, 1$ (light green, left and dark green, right) taken at the boundary of the spatial domain in the respective kymographs. Kymographs representing the spatiotemporal evolution of cyclin B-Cdk1. Starting from a spatially homogeneous initial condition of activity and a spatially heterogeneous period dependence to introduce a pacemaker exhibiting trigger waves for high α (Middle). Starting from a spatially linear phase difference in the initial condition of activity and a spatially homogeneous period exhibiting phase waves independently of α (Bottom). (B) Temporal evolution with cycle number of the spatially averaged wave speed for phase and trigger waves in the shown kymographs. (C) v and γ as function of α resulting from fitting the last wave in the numerical simulations with the expression $x = d + vt^{\gamma}$ showing the progressive transition from linearly propagating trigger waves.

Discussion

Due to the complexity of living matter, communication and coordination of bioprocesses is of utmost importance. From patterns of firing neurons to the flocking of birds, biological systems demonstrate this necessity on a regular basis. In this work, we probed the behavior and nature of one such coordination mechanism: mitotic waves that coordinate the process of cell division in large cells. Using a frog extract system which reproduces cell cycles *in vitro*, we characterized how mitosis spreads through the *Xenopus laevis* cytoplasm via either phase waves or trigger waves.

Phase waves are phase-shifted oscillations of the bulk medium that give the illusion of a propagating wave, and hence they are also called pseudo waves or kinematic waves (31,32). The velocity of these phase waves is directly determined by the initial phase gradient. Shallow gradients --- when the system is initialized approximately at the same time throughout space --- lead to phase waves that propagate very fast. Phase waves are typically not greatly altered by diffusion, and they do not require such spatial interactions. *Trigger waves*, however, only exist in the presence of spatial coupling (10–12,31,33). They represent a dynamical attracting solution in the system with a well-defined velocity and amplitude. Trigger waves do not slow down or lose amplitude as they travel.

Although properties of trigger waves have been elaborately studied in the literature (20,21,33–37), the transient system dynamics as one approaches the attracting trigger wave solution are typically not looked at. Yet, arguably all biological processes are continuously in transient, so it is crucial to look into how coordination through wave phenomena occurs in transient. Through our frog egg extract experiments in thin long (quasi-one-dimensional) tubes, we observed phase waves in the transient dynamics towards the formation of a stable trigger wave. Even though at the same time cell cycle oscillations slowed down as well, we showed that this is not required to observe a transition from phase waves to trigger waves. Certainly, in oscillatory media it can take a long time before a pacemaker, a region that oscillates faster than its surroundings, is able to entrain its surroundings via trigger waves (20,21). While in excitable media, a trigger wave can travel uninterrupted throughout the medium, in oscillatory media the distance it can entrain is limited by the inherent oscillatory period of its surroundings. Even in the transient time when a trigger wave is still forming, the regular biochemical oscillations that drive the early embryonic cell cycle in *Xenopus laevis* will drive the whole system into mitosis throughout the whole medium. Any phase gradients will thus give rise to phase waves, which were also dubbed “sweep waves” recently (16), as the cell cycle phase is swept up.

This puts our work in dialogue with the existing literature regarding mitotic waves in *Drosophila*. Although period lengthening was found to be a driver of a sweep-to-trigger transition in *Drosophila (17)*, we showed that this is not required for directing a transition from phase waves to trigger waves. Furthermore, this and other work highlight that phase wave properties are not robust to heterogeneity as they do not correspond to an actual attracting system solution. In Hayden et al. *(17)*, the authors also perform experiments and simulations with embryos displaying a heterogeneous distribution of nuclei in the syncytial embryo. They remark that disrupting homogeneity leads to trigger waves and a loss of synchrony. We demonstrate a similar effect both by adding nuclei to the homogenous system, and by driving it explicitly with CSF. In all three cases, these trigger-wave-producing effects overtake underlying quasi-synchronous patterns. As phase waves do not actively propagate through a medium and require structured initial phase

differences over a certain distance, they typically only persist for hundreds of microns. A trigger wave can travel long distances (~10 mm), and the typical length scale of the concentration gradient at the leading front ranges around hundreds of microns as well. This underscores the prevalence of phase waves in relatively small embryos, such as Drosophila, due to the limited length to accommodate a trigger wave front gradient in reduced size embryos. On the scale of some biological functions, the propagation distance of phase waves is relevant. However, for the specific purpose of coordinating function, this seems insufficient in larger cells. Trigger waves, as made evident by our work here, conversely, transmit signals orders of magnitude farther in distance. This questions the physiological relevance of phase waves. At most, one could argue for a tradeoff between speed and distance. For mitosis it could be reasonable that nature would select for trigger waves in larger embryos such as *Xenopus*, where coordinating over large distances is more relevant than in *Drosophila*. Recently reported ultrafast waves (10,16,38,39), faster-than-trigger-wave signaling achieved without requiring bistable reactions or diffusion-mediated coupling, necessitate further comprehensive studies to understand the fundamental nature of these waves in comparison to classical trigger waves. Our work highlights the importance of examining not only stable waves but also the time evolution of waves as they develop. It also provides a framework that integrates experiments and theory to dissect the transition between different wave regimes.

Moreover, recent works in frog egg extracts have shown that nuclei might act as pacemakers for generating trigger waves (13,14). Here, by studying very large spatial systems (tubes of multiple millimeters long), we examined the transient dynamics of many interacting pacemaker regions. In the absence of nuclei, smaller heterogeneities in the cytoplasm were able to slowly develop various pacemaker regions sending out trigger waves. This transient time was greatly reduced when introducing multiple nuclei in the system and/or driving the system with CSF extract from the boundary. Our work provides rare experimental analysis of the transient dynamics of multiple interacting pacemakers. Theoretically, it has been shown that when multiple pacemakers in the same medium compete, the strongest pacemaker ends up entraining the whole medium (40,41). The strength of a pacemaker is determined by its size and the period difference with the surrounding medium, as well as the nature of the medium itself (40,41).

Future experiments could expand on this work by pursuing other forms of perturbations by inhibiting the feedback loops in the network. The field already demonstrated the importance of Wee1 for “forming the trigger” (8), but with our setup and analysis framework, one could quantify the effect and provide stronger evidence in either direction. The same applies to Cdc25, a phosphatase acting antagonistically to the Wee1 kinase in the regulation of Cdk1, both forming positive feedback loops with Cdk1. It would be interesting to observe whether Wee1 and Cdc25 affect this time dependence in similar manners. Moreover, we know that these inputs also translocate in and out of the nucleus throughout one cycle, at different times (42,43). It stands to reason that inhibition thereof could change in the presence of nuclei, and thus, we might see a nuclei-dependent effect on how inhibition perturbs this transition. Clearly, much work remains on elucidating the details of time-dependent wave behavior.

Additionally, we demonstrated the use of the CSF driving setup to offer a mechanistic way of probing mitotic trigger waves directly. In the future, this system could be used to expand on this study by asking how perturbations to the clock, including inhibitors for other clock constituents such as Cdc25, Wee1, PP2A, and many others, change trigger wave propagation. Furthermore, like CSF extracts, interphase extracts maintain activity for months while frozen, making them more accessible for faster and simpler data acquisition than involving the cycling system. In practice, such experiments could provide a more

straightforward method for testing all of the perturbations mentioned above: clock inhibitors, glycerol (diffusion), etc. In particular, this would allow for a direct examination of whether nuclei actually perturb wave propagation as it would eliminate their dual role as a pacemaker. In total, this setup offers a wealth of opportunities to probe trigger wave dynamics, relevant for *in vivo* embryogenesis in *Xenopus*.

Additionally, one can imagine perturbing the source itself. Theory predicts the wave speed to depend on the difference between the pacemaker and bulk frequency (20,21). Either through dilution or inhibitors, it is plausible that the driving frequency of the CSF source could be modulated, thus providing a direct test of these theoretical predictions. Admittedly, the interplay between CSF arrest and its driving force is not known, so it is likely this set of perturbations would be more complicated to explain. Accurate modeling work could assist with this. Nevertheless, as we have demonstrated the efficacy of driving waves in vitro, understanding this interaction is important. Taken together, this future work would help further solidify the field's detailed knowledge of how organisms transmit mitotic information across great lengths, but also provide fundamental information regarding the nature of biochemical waves generally, and phase waves and trigger waves in particular.

Materials and Methods

Extracts

To capture mitotic waves in vitro, we made cell-free cycling extracts from *Xenopus laevis* eggs following a published protocol (Figure 1, A) (25) with one main modification (18). Extracts were then supplemented with various reporters, drugs and/or sperm DNA, depending on the experimental conditions desired. Work from the Yang lab demonstrated increased dilution can improve the number of cycles, with the best activity coming around 20% dilution (44). As a result, for the data described here, the dilution is kept constant at 20% with extract buffer (100 mM KCl, 0.1 mM CaCl2, 1 mM MgCl2, 10 mM potassium HEPES, 50 nM sucrose, pH 7.8). Regardless of this fact, extracts were subsequently loaded into long 5-10 mm-long sections of Masterflex PTFE tubing (inner diameter 150 μm) via aspiration, submerged under mineral oil, and then recorded using time-lapse epifluorescent microscopy [Olympus IX-83]. Given the dimensions of the tubing used, tubes were organized into, at most, groups of five in one direction. We did not observe any significant contamination between tubes, even when forcing them into such close proximity. The Cdk1-FRET sensor is as described in Maryu and Yang (15).

The CSF extracts were made following established protocols (28) which are minimally adapted from the originals (25). Using laid eggs, we produced large quantities of extract (on the order of mL), vastly more than necessary for a single experiment (10-20 μL). To preserve said large quantities of extract, we implemented a freezing protocol adopted from Takagi and Shimamoto (29) .

On the day of an experiment, one aliquot of each CSF fraction is allowed to thaw on ice, and when combined, are ready to be used. To maintain conditions across the reservoir and the cycling extract, CSF extracts were also diluted to 20% with extract buffer. No reporters or drugs were added. We cut PTFE tubing into individual sections of ~10mm lengths and loaded each via aspiration such that the extract filled the tube in excess: visual inspection of the syringe adapter showed the fluid line exceeding the tube opening. Then the tube was dipped into the CSF reservoir syringe-end first for 5-10 seconds to ensure fluidic contact between the cycling and CSF extracts. While the original apoptotic wave paper described maintaining contact between the reservoir and tubes for many minutes, we observed any contact longer than ~10 seconds resulted in mitotic arrest overtaking most, if not all, of the tube (23). In fact, even at short dipping times, this sometimes occurred regardless. As such, care was taken to minimize the contact time.

Image Processing and Analysis methods

Grids of images were captured and subsequently stitched together using ImageJ's Grid/Pairwise Stitching plug-in (45), in conjunction with additional pipeline code written in Fiji/Java. Bright-field images from the first frame were used to generate stitching parameters, then fed these parameters to ImageJ to stitch each channel at each frame consecutively. While capturing grids of images in this way results in a non-zero timestep between subsequent sections along a tube—and thus, some multiple of this dt between the first and last sections—this gap amounts to a few seconds, much smaller than the scale of the overall imaging timestep which is on the order of minutes. As such, this can be and is ignored for the purposes of analysis. The stitched stacks are then straightened using Fiji and a manually selected curve from the bright-field images as an input. This curve is unique to each tube, though the profiles of the tubing sections often followed roughly the same shape, so not much distortion is expected. Afterwards, the tubes are cropped so

as to only include the inner dimension, again using the bright-field images as a guide. Additionally, calculation of the FRET ratio is handled separately as given in Maryu and Yang (15).

For the analysis of wavefronts, first, individual kymographs are corrected for any decaying baseline trend, and any NaN pixels are filled using the scikit-image function inpaint. Afterwards, we detect peaks for each time series at each pixel along the tube. The peaks themselves are then clustered into individual cycles in Python. Once cycles are identified and separated, the collection(s) of peaks are fitted and/or smoothed in space and time, after which slopes (and speeds) are calculated along each front by taking the numerical derivative of the fits at each point. Periods follow directly from the detected peaks. The normalized density estimation for the time dependence of the period, $\frac{dA}{dt}$, and slope makes use of the Scipy function scipy.stats.gaussian_kde using a Gaussian kernel of $\sigma_t = 50\ min$ as a sliding window for time and the maximum value normalized to one.

Mathematical model

We use the mathematical model previously introduced (8,19) describing the dynamics of the total cyclin B – Cdk1 $c \equiv c(x,t)$ and its active form $a \equiv a(x,t)$. The equations can be written in the following form:

$$\partial_t c = \tau\, \beta\, (\, k_s - h_{Deg}(a)c) + D\nabla^2 c, \qquad (1)$$

$$\partial_t a = \tau\, [\alpha\, (h_{Cdc25}(a)(c-a) - h_{Wee1}(a)a) + \beta(\, k_s - \beta h_{Deg}(a)a)] + D\nabla^2 a, \qquad (2)$$

where the newly introduced dimensionless parameters are α, β, τ. The parameter τ scales all parameter rates and allows for precise control of the period of the oscillations. The parameter α scales the rates related to activation-inactivation processes mediated by Cdc25 phosphatase and Wee1 kinase, which are described by Hill functions of the form $h_{Cdc25}(a) = a_{Cdc25} + b_{Cdc25} a^{n_{Cdc25}}/({EC_{50,Cdc25}}^{n_{Cdc25}} + a^{n_{Cdc25}})$, , $h_{Wee1}(a) = a_{Wee1} + b_{Wee1} {EC_{50,Wee1}}^{n_{Wee1}}/({EC_{50,Wee1}}^{n_{Wee1}} + a^{n_{Wee1}})$. The parameter β scales synthesis and degradation rates to control the time spent in interphase and mitosis. The degradation term encompasses the APC/C-induced degradation of cyclin B which is described with the hill function $h_{Deg}(a) = a_{Deg} + b_{Deg} a^{n_{Deg}}/({EC_{50,Deg}}^{n_{Deg}} + a^{n_{Deg}})$. The parameters of the model are $k_s = 1.5\,\frac{nM}{min}, a_{Cdc25} = 0.8\ min^{-1}, b_{Cdc25} = 4\ min^{-1},\ EC_{50,Cdc25} = 35\ nM, n_{Cdc25} = 11, a_{Wee1} = 0.4\ min^{-1},\ b_{Wee1} = 2\ min^{-1},$ $EC_{50,Wee1} = 30\ nM, n_{Wee1} = 3.5, a_{Deg} = 0.01\ min^{-1},\ b_{Deg} = 0.06\ min^{-1},\ EC_{50,Deg} = 32\ nM, n_{Deg} = 17, D = \frac{240\ \mu m^2}{min},\ \alpha, \beta, \tau = 1$ and are kept constant in this work otherwise specified.

Numerical simulations

The model described by Eq. (1) and (2) is a system of two coupled partial differential equations (PDEs) which is integrated in time with a pseudo-spectral method (46). We consider a grid with N_x grid points to describe a spatial domain of length L_x with no-flux boundary conditions and we integrate with a timestep Δt the linear terms in Fourier space exactly, while the nonlinear terms are integrated using a second-order in time approximation.

Numerical simulations showing the transition from phase to trigger waves in time (Fig. 2B, C(i)-(ii)) have been performed using the integration parameters N_x= 4096, L_x= 10 mm and $\Delta t = 0.002$ starting with an initial condition of $a(x) = i(x) = 0$ introducing spatial heterogeneity in the synthesis term of the following

form: $k_s(x) = k_s\left(1 + P(x) + A_{k_s}N(x)\right)$, where $P(x)$ is a manually introduced profile to induce pacemakers at chosen locations for visualization porpoises in Fig. 2B and set to zero in panels (i) and (ii) of Fig. 2C to explore the dependence with synthesis noise amplitude A_{k_s}. The introduced heterogeneity $N(x)$ is computed by generating colored noise $\mathcal{N}(x) = F^{-1}[e^{-\frac{(\sigma k)^2}{2} - 2i\pi u_k}](x)$ using the inverse Fourier transform F^{-1} where is u_k is a random number uniformly distributed between 0 and 1 for each Fourier mode k and the typical length scale of the spatial heterogeneities is chosen $\sigma = 77.46\ \mu m$. The noise is later normalized to have a maximum value of one with the expression, $N(x) = (\mathcal{N}(x) - \frac{\int_0^{L_x}\mathcal{N}(x)dx}{L_x})/max(\mathcal{N}(x) - \frac{\int_0^{L_x}\mathcal{N}(x)dx}{L_x})$. The temporal dependence $\beta(t)$ is computed using the linear dependence of the period $T(1/\beta)$ shown in Fig. 2A (middle) to reproduce the experimental dependence of the period with time extracted from Fig. 1D. The calculated $\beta(t)$ is initialized at the time of the second oscillation t_{o2} which corresponds to the first measurement of the period in the experiments.

Numerical simulations in panels (i)-(ii) of Fig. 2C and those used for the calculation of the theoretical dispersion relation in Fig. 2D (black dashed) have been performed using the integration parameters N_x= 512, L_x=10 mm and $\Delta t = 0.002$ starting with an initial condition of $a(x) = i(x) = 0$ introducing a pacemaker at the center using a step function for $\tau(x) = 1 + \Delta\tau\, H(s/2 - |x - L_x/2|)$ = where $\Delta\tau = 0.5$, $H(x)$ is the Heaviside function, $s = 20\ \mu m$ is the size of the introduced pacemaker and changing the background period with the parameter β.

Numerical simulations in Fig. 5 have been performed using the integration parameters N_x= 1024, L_x= 5 mm and $\Delta t = 0.002$ starting with an initial condition of $a(x) = i(x) = 0$ introducing a pacemaker at the center using a step function for $\tau(x)$ as previously introduced with $\Delta\tau = 0.3$, and $s = 50\ \mu m$ for simulations showing trigger waves. Simulations showing phase waves use a constant value of τ and as initial condition for $a(x) = \frac{2(a_{min} - a_{max})}{L_x}|x - L_x/2| + a_{min}$ a linear triangular spatial profile of decreasing activity from $a_{max} = 20$ to $a_{min} = 0$ as the distance from the center increases. $i(x)$ can be computed by making use of the fact that a relaxation oscillator moves close to the folded nullcline. Thus using the nullcline resulting from Eq. (1) equal to zero on can compute $i(x) = c_{nullcline}(a(x)) - a(x)$, where $c_{nullcline}$ is the total cyclin B, $c = a + i$ along the nullcline.

References

1. Novak B, Tyson JJ. Numerical analysis of a comprehensive model of M-phase control in Xenopus oocyte extracts and intact embryos. J Cell Sci. 1993;106 (Pt 4:1153–68.

2. Novak B, Tyson JJ. Modeling the cell division cycle: M-phase trigger, oscillations, and size control. J Theor Biol. 1993;165:101–34.

3. Morgan D. Cell Cycle: Principles of Control [Internet]. 2008/02/. New Science Press: London.; 2007. Available from: https://www.ncbi.nlm.nih.gov/pmc/articles/PMC2248297/

4. Foe VE, Alberts BM. Studies of nuclear and cytoplasmic behaviour during the five mitotic cycles that precede gastrulation in Drosophila embryogenesis. J Cell Sci. 1983;61:31–70.

5. Hara K, Tydeman P, Kirschner M. A cytoplasmic clock with the same period as the division cycle in Xenopus eggs. Proc Natl Acad Sci U S A. 1980;77(1):462–6.

6. Farrell JA, O'Farrell PH. From egg to gastrula: how the cell cycle is remodeled during the Drosophila mid-blastula transition. Annu Rev Genet. 2014;48:269–94.

7. Anderson GA, Gelens L, Baker JC, Ferrell JE. Desynchronizing Embryonic Cell Division Waves Reveals the Robustness of Xenopus laevis Development. CellReports. 2017;21:37–46.

8. Chang JB, Ferrell JE. Mitotic trigger waves and the spatial coordination of the Xenopus cell cycle. Nature. 2013;500(7464):603–7.

9. Deneke VE, Melbinger A, Vergassola M, Di Talia S. Waves of Cdk1 Activity in S Phase Synchronize the Cell Cycle in Drosophila Embryos. Dev Cell. 2016;38(4):399–412.

10. Deneke VE, Di Talia S. Chemical waves in cell and developmental biology. J Cell Biol. 2018;217(4):1193–204.

11. Gelens L, Anderson GA, Ferrell JEJ. Spatial trigger waves: positive feedback gets you a long way. Mol Biol Cell. 2014;25(22):3486–93.

12. Di Talia S, Vergassola M. Waves in Embryonic Development. Annu Rev Biophys. 2022;51(1):327–53.

13. Nolet FE, Vandervelde A, Vanderbeke A, Piñeros L, Chang JB, Gelens L. Nuclei determine the spatial origin of mitotic waves. eLife. 2020;9:e52868.

14. Afanzar O, Buss GK, Stearns T, Ferrell Jr JE. The nucleus serves as the pacemaker for the cell cycle. eLife. 2020;9:e59989.

15. Maryu G, Yang Q. Nuclear-cytoplasmic compartmentalization of cyclin B1-Cdk1 promotes robust timing of mitotic events. Cell Rep. 2022;41(13):111870.

16. Vergassola M, Deneke VE, Talia SD. Mitotic waves in the early embryogenesis of *Drosophila*: Bistability traded for speed. Proc Natl Acad Sci U S A 2018;115(10):E2165–74.

17. Hayden L, Hur W, Vergassola M, Di Talia S. Manipulating the nature of embryonic mitotic waves. Curr Biol CB. 2022 Nov 21;32(22):4989-4996.e3.

18. Guan Y, Li Z, Wang S, Barnes PM, Liu X, Xu H, et al. A robust and tunable mitotic oscillator in artificial cells. eLife. 2018;7:e33549.

19. Yang Q, Ferrell JE. The Cdk1-APC/C cell cycle oscillator circuit functions as a time-delayed, ultrasensitive switch. Nat Cell Biol. 2013;15(5):519–25.

20. Rombouts J, Gelens L. Synchronizing an oscillatory medium: The speed of pacemaker-generated waves. Phys Rev Res. 2020;2(4):43038.

21. Rombouts J, Gelens L. Analytical approximations for the speed of pacemaker-generated waves. Phys Rev E. 2021 Jul;104(1–1):014220.

22. Nolet FE, Gelens L. Mitotic waves in an import-diffusion model with multiple nuclei in a shared cytoplasm. Biosystems. 2021;208:104478.

23. Cheng X, Ferrell JEJ. Apoptosis propagates through the cytoplasm as trigger waves. Science. 2018 Aug 10;361(6402):607–12.

24. Masui Y, Markert CL. Cytoplasmic control of nuclear behavior during meiotic maturation of frog oocytes. J Exp Zool. 1971 Jun;177(2):129–45.

25. Murray AW. Cell Cycle Extracts. Methods Cell Biol. 1991;36:581–605.

26. Schmidt A, Rauh NR, Nigg EA, Mayer TU. Cytostatic factor: an activity that puts the cell cycle on hold. J Cell Sci. 2006 Apr;119(7):1213–8.

27. Yamamoto TM, Iwabuchi M, Ohsumi K, Kishimoto T. APC/C–Cdc20-mediated degradation of cyclin B participates in CSF arrest in unfertilized Xenopus eggs. Dev Biol. 2005;279(2):345–55.

28. Good MC, Heald R. Preparation of Cellular Extracts from Xenopus Eggs and Embryos. Cold Spring Harb Protoc. 2018 Jun 1;2018(6).

29. Takagi J, Shimamoto Y. High-quality frozen extracts of Xenopus laevis eggs reveal size-dependent control of metaphase spindle micromechanics. Mol Biol Cell. 2017 Aug 1;28(16):2170–7.

30. Deming P, Kornbluth S. Study of apoptosis in vitro using the Xenopus egg extract reconstitution system. Methods Mol Biol Clifton NJ. 2006;322:379–93.

31. Winfree AT. The Timing of Biological Clocks. Scientific American Books, Inc.; 1986.

32. Bordiougov G, Engel H. From trigger to phase waves and back again. Phys Nonlinear Phenom. 2006;215(1):25–37.

33. Tyson JJ, Keener JP. Singular perturbation theory of traveling waves in excitable media (a review). Phys Nonlinear Phenom. 1988;32(3):327–61.

34. Elphick C, Hagberg A, Malomed BA, Meron E. On the origin of traveling pulses in bistable systems. Phys Lett A. 1997 Feb;230(1):33–7.

35. Hagberg A, Meron E. Pattern formation in non-gradient reaction-diffusion systems: The effects of front bifurcations. Vol. 7, Nonlinearity. 1994. p. 805–35.

36. Rinzel J, Terman D. Propagation Phenomena in a Bistable Reaction-Diffusion System. SIAM J Appl Math. 1982;42(5):1111–37.

37. Bode M. Front-bifurcations in reaction-diffusion systems with inhomogeneous parameter distributions. Phys Nonlinear Phenom. 1997;106(3):270–86.

38. Puls O, Yang Q. The Rise of Ultrafast Waves. Dev Cell. 2018 Dec 3;47(5):532–4.

39. Wu Z, Su M, Tong C, Wu M, Liu J. Membrane shape-mediated wave propagation of cortical protein dynamics. Nat Commun. 2018 Jan 10;9(1):136.

40. Stich M, Mikhailov AS. Complex Pacemakers and Wave Sinks in Heterogeneous Oscillatory Chemical Systems. 2002;216(4):521.

41. Nolet FE, Rombouts J, Gelens L. Synchronization in reaction–diffusion systems with multiple pacemakers. Chaos Interdiscip J Nonlinear Sci. 2020 May;30(5):053139.

42. Baldin V, Ducommun B. Subcellular localisation of human wee1 kinase is regulated during the cell cycle. J Cell Sci. 1995 Jun;108 (Pt 6):2425–32.

43. Trunnell NB, Poon AC, Kim SY, Ferrell JE. Ultrasensitivity in the Regulation of Cdc25C by Cdk1. Mol Cell. 2011;41(3):263–74.

44. Jin M, Tavella F, Wang S, Yang Q. In vitro cell cycle oscillations exhibit a robust and hysteretic response to changes in cytoplasmic density. Proc Natl Acad Sci U S A. 2022 Feb 8;119(6).

45. Preibisch S, Saalfeld S, Tomancak P. Globally optimal stitching of tiled 3D microscopic image acquisitions. Bioinforma Oxf Engl. 2009 Jun 1;25(11):1463–5.

46. Montagne R, Hernández-García E, Amengual A, San Miguel M. Wound-up phase turbulence in the complex Ginzburg-Landau equation. Phys Rev E. 1997 Jul;56(1):151–67.

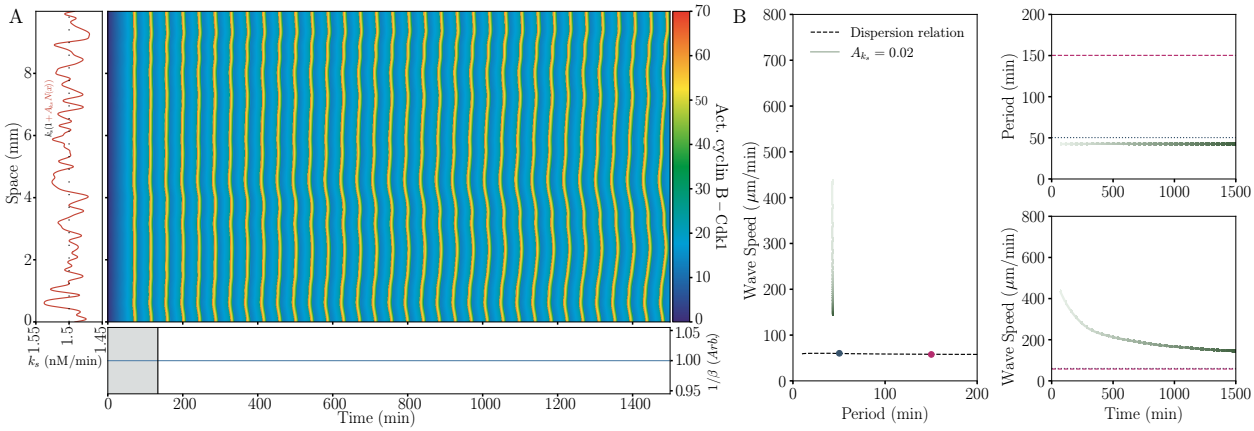

Figure S1: Spatiotemporal evolution of the activity of cyclin B-Cdk1 showing the transition from phase to trigger waves with constant period with time using the parameter $\beta(t)$=1 (bottom) and spatial variability in the synthesis term $k_s(x)$. (B) Dispersion relation and temporal dependence of the period and wave speed of the numerical simulation in (A), and the theoretical dispersion relation using the parameter β to scan the period (black dashed line) same as in Fig. 2 included for comparison.

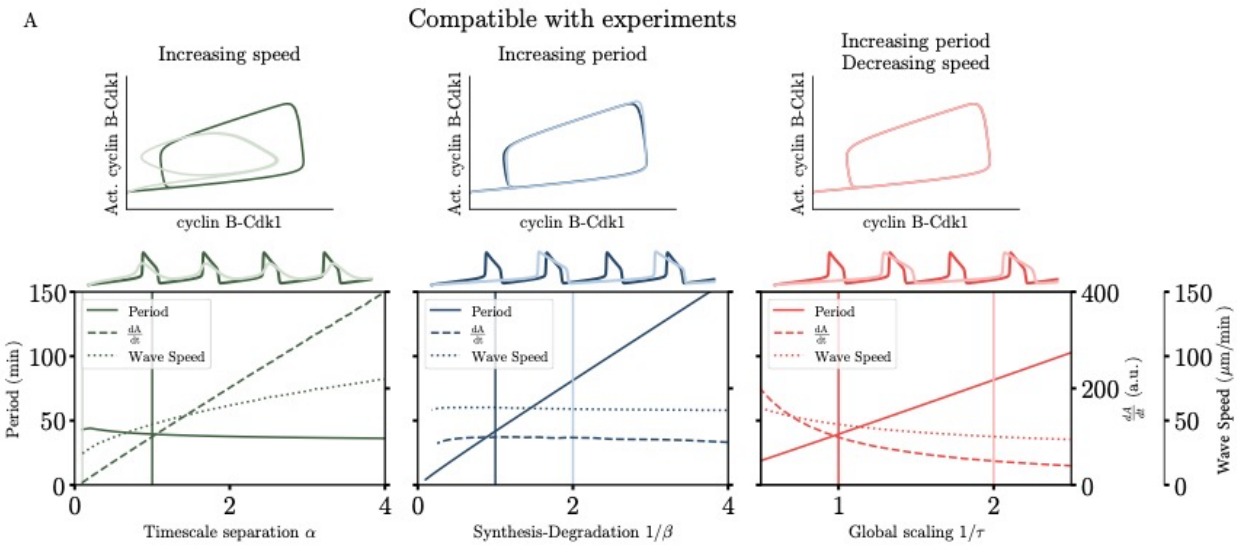

Figure S2: Dependence on the period, $\frac{dA}{dt}$ and wave speed for different parameter scalings. Top: Phase space representation of the oscillator and the corresponding time series. Bottom: Period, $\frac{dA}{dt}$ and wave speed is represented using continuous, dashed and dotted lines as function of timescale separation α (left), decreasing synthesis and degradation rates with β (center), and all rates with τ (right). Vertical lines indicate the parameter values used in the top panels with the respective colors